UDK 67.017:669.721.5:621.791.318
Original scientific article/Izvirni znanstveni članek

ISSN 1580-2949
MTAEC9, 52(4)487(2018)

CHARACTERIZATION OF AZ31B MAGNESIUM ALLOY JOINTS WELDED WITH A Nd:YAG LASER

KARAKTERIZACIJA ZVARNEGA SPOJA MAGNEZIJEVE ZLITINE AZ31B, IZDELANEGA Z Nd:YAG LASERJEM

Hongtao Liu[1], Jixue Zhou[1], Yanfei Chen[2], Tao Li[2], Xuebing Jiao[3], Yuansheng Yang[4], Tao Lin[2], Kaiming Cheng[1]

[1]Shandong Key Laboratory for High Strength Lightweight Metallic Materials, Advanced Materials Institute, Shandong Academy of Sciences, Jinan 250014, China
[2]Shandong Engineering Research Center for Lightweight Automobiles Magnesium Alloys, Advanced Materials Institute, Shandong Academy of Sciences, Jinan 250014, China
[3]College of Material Science and Engineering, Shandong Jianzhu University, Jinan 250101, China
[4]Institute of Metal Research, Chinese Academy of Sciences, Shenyang 110016, China
kelekm73@163.com

Prejem rokopisa – received: 2017-10-26; sprejem za objavo – accepted for publication: 2018-02-15

doi:10.17222/mit.2017.180

In the present study, an AZ31B magnesium alloy was welded using a low-power pulsed Nd:YAG laser attached to a six-axis welding robot. The welding metallurgical characteristics, including microstructure, porosity formation, texture evolution and microhardness distribution were systematically investigated using a scanning electron microscope (SEM), electron backscatter diffraction (EBSD) and a microhardness tester. The transverse cross-sectional microstructure of the AZ31B-alloy joint was composed of the base metal (BM), columnar-grain zone (CGZ) and equiaxed-grain zone (EGZ) in the center of the fusion zone (FZ). Some pores were observed in the FZ and believed to be related to the pre-existing pores in the BM. Especially, it was noted that many columnar grains observed in the transverse cross-section of the FZ were almost perpendicular to the solid-fusion boundary. Nevertheless, a large number of fine equiaxed grains formed on the top surface of the FZ and exhibited obvious random orientations. Different grain-growth mechanisms found on the transverse cross-section and the top surface of the weld bead were empirically investigated. Owing to apparent grain coarsening, the lowest microhardness value (~ 43 HV) was detected in the center of the FZ, which was evidently lower than that of the BM (~ 68 HV).

Keywords: AZ31B magnesium alloy, Nd:YAG laser welding, microstructure, pores, texture, electron backscatter diffraction

Avtorji študije so magnezijevo zlitino AZ31B varili s pulznim Nd:YAG laserjem nizke moči, nameščenem na šestosnem varilnem robotu. Sistematično so izvedli metalurško karakterizacijo varjenja, vključno z analizo mikrostrukture, analizo tvorbe poroznosti in razvoja teksture s pomočjo vrstične elektronske mikroskopije (SEM) v kombinaciji s sipanjem povratnih elektronov (EBSD). Porazdelitev mikrotrdote po preseku zvara so določili z merilnikom mikrotrdote. Posnetki mikrostrukture v prečnem preseku zvarnega spoja zlitine AZ31B so pokazali, da je le ta sestavljen iz osnovne kovine (BM; angl.: base metal), cone stebričastih kristalnih zrn (CGZ; angl.: columnar grains zone), cone enakoosnih zrn (EGZ; angl.: equiaxed grains zone) in centralne staljene cone (FZ, angl.: fusion zone). V FZ so opazili tudi nekaj por in avtorji verjamejo, da je to posledica predhodno obstoječih por v BM. Še posebej poudarjajo opažanje, da se mnoga stebričasta zrna nahajajo v prečnem preseku FZ , ki so skoraj pravokotna na fazno mejo trdno-talina. Kakorkoli, na vrhu površine FZ se nahaja veliko število tvorjenih drobnih enakoosnih kristalnih zrn z očitno naključno orientacijo. Avtorji prispevka empirično razpravljajo v članku tudi o različnih mehanizmih rasti zrn med prečnim presekom in vrhom površine varilne posteljice (bazenčka staljene kovine). Zaradi jasne rasti zrn so najmanjšo mikrotrdoto (~ 43 HV) izmerili v centru FZ, kar je očitno precej manj kot v BM (~ 68 HV).

Ključne besede: magnezijeva zlitina AZ31B, varjenje z Nd:YAG (Neodim:Itrij-Aluminijev granat) laserjem, mikrostrukture, pore, teksture, sipanje povratnih elektronov

1 INTRODUCTION

Being promising structural metallic materials, magnesium alloys have gained increased interest in the automotive and aircraft industries for their light weight, good electromagnetic shielding, and excellent castability.[1–3] However, the poor formability and cold processability of magnesium alloys restrict their widespread engineering applications. This is because magnesium has a hexagonal close-packed (HCP) crystal structure that cannot activate enough slip systems at room temperature. Therefore, the high-performance welding technologies are essential for further expanding the application fields of Mg alloys. Various welding technologies have been applied to weld Mg alloys, such as tungsten-inert-gas (TIG) welding,[4,5] laser-beam welding (LBW),[6,7] laser-arc hybrid welding,[8] and friction-stir welding (FSW).[9]

Among these welding methods, LBW is suitable to weld magnesium alloys for its remarkable advantages, including low residual stress, high-power density and large depth-to-width ratio.[10,11] After the laser welding, the solidification in the fusion zone (FZ) produces significant microstructural changes. The reliability of a welded joint depends strongly on the microstructural changes in the FZ and the base material (BM) after the welding.[12] Nevertheless, limited work regarding the microstructure including the porosity origin, grain-growth

mechanism and texture evolution after the LBW of magnesium alloys has been reported.

Therefore, laser welding of AZ31B Mg alloys was performed in the present study, using a low-power pulsed Nd:YAG laser attached to a six-axis welding robot. The solidification microstructure, grain growth, porosity formation, texture evolution and microhardness distribution were systematically investigated to understand the metallurgical characteristics of an automatic-laser-welded AZ31B alloy joint.

2 EXPERIMENTAL PART

In the present study, 2-mm-thick as-rolled AZ31B Mg alloy sheets were selected for laser welding; their chemical composition in weight percent is listed in **Table 1**. Before the laser welding, the AZ31B alloy sheets were cleaned with acetone to remove grease and then polished with SiC papers to remove oxides. As shown in **Figure 1**, a low-power pulse Nd:YAG laser attached to a six-axis robot was employed for the welding research. The laser butt welding was performed on an AZ31B specimen under the conditions of 600 W laser power, 9.2 mm/s welding speed, and 600 μm focused beam spot. During the laser-welding process, the argon shielding gas was ejected to protect the top and bottom surfaces at 15 L/min and 20 L/min, respectively.

Table 1: Chemical composition of the AZ31B sheets, in mass fractions (*w*/%)

Al	Zn	Mn	Fe	Si	Cu	Mg
3.15	1.00	0.29	<0.003	<0.01	<0.001	Balance

After the laser welding, the welded joint was aged at 473 K for 1 h. The microstructures of weld samples were examined with optical microscopy (OM) and scanning electron microscopy (SEM) after mechanical polishing and subsequent etching in a corrosive solution of 4.2 g picric acid, 70 mL ethanol, 10 mL glacier acetic and 10 mL deionized water. SEM observations were conducted using a Zeiss EVO MA10 SEM in the second electron detection mode at 20 kV.

For EBSD mapping and a texture analysis of the joint, EBSD measurements were performed under the conditions of 20 kV electron beam, 10 nA probe current, 17 mm working distance, 20 ms integration time and 0.5 μm step size. The EBSD specimens were first mechanically polished, followed by electrolytic polishing in a commercial AC2 solution at 16 V for 80 s at –15 °C. Electron backscatter diffraction (EBSD) was done using SEM (Zeiss EVO MA10) together with a Nordlys-S detector, a CCD camera, the HKL data-acquisition software and the Channel 5.0 post-processing-analysis software package. The obtained EBSD map covered the BM and the FZ of the welded specimen. To analyze the texture evolution, pole figures were produced from the EBSD map of the BM and FZ.

A Huayin HV-1000 type microhardness tester was used to measure the Vikers microhardness across the seam after the specimen was polished. A 200-g load and 20-s dwell time were applied for the hardness tests. An adequate space was retained to avoid interaction effects between the adjacent indentations, and three measurements were taken to determine the error bars.

3 RESULTS AND DISCUSSION

3.1 Appearance and microstructure

A macro seam appearance is an important evidence of the welding qualities. As observed in **Figure 2**, a smooth, uniform and regular fish-scale pattern of the seam was observed on the weld surface. The top and bottom widths of the welding bead were about 2 mm and 1 mm, respectively. Moreover, no welding defects, such as cracks, incomplete fusion or slag inclusion were found.

The typical microstructure of the transverse cross-section of the AZ31B laser weld is shown in **Figure 3**. This joint microstructure can be divided into three zones with different microstructural features, including BM, columnar-grain zone (CGZ) near the fusion boundary, and equiaxed-grain zone (EGZ) in the center of the FZ.

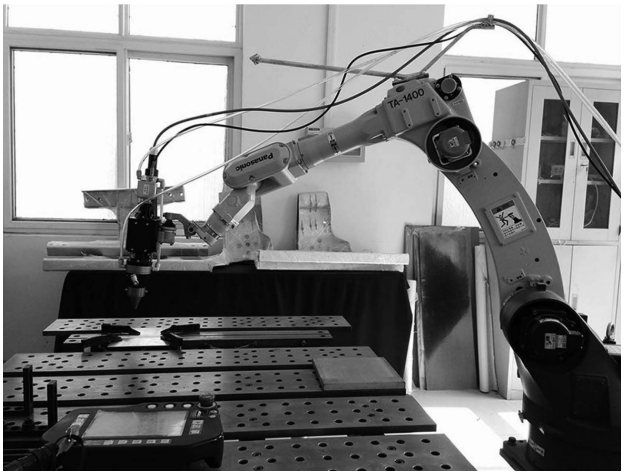

Figure 1: Nd:YAG laser-equipped six-axis robot

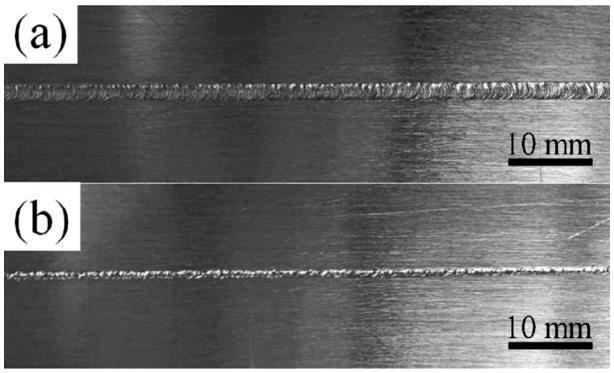

Figure 2: Appearance of the AZ31B laser seam: a) top surface, b) bottom surface

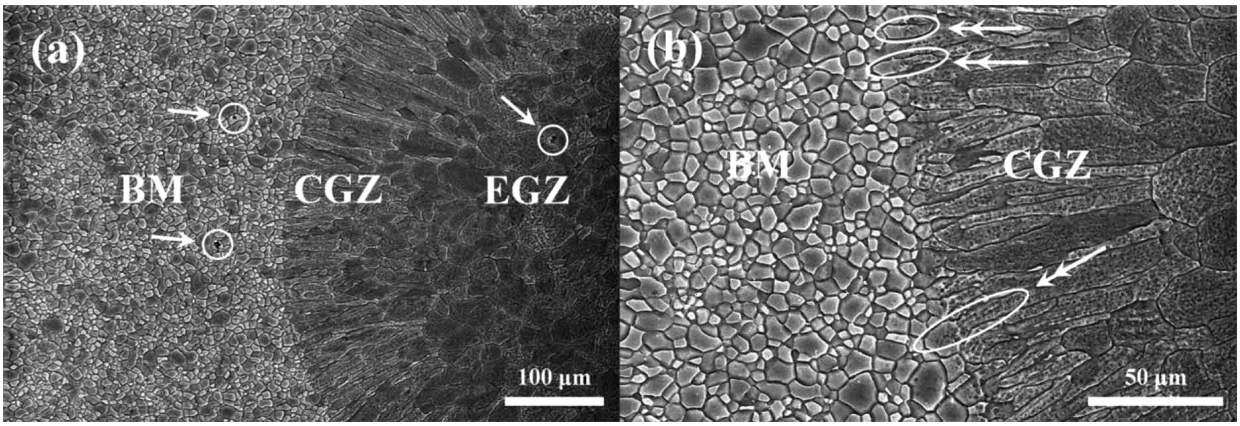

Figure 3: a) Cross-sectional microstructure of the laser-welded AZ31B joint, b) larger magnification of the cross-section

Owing to the low heat input during the laser welding, no apparent heat-affected zone (HAZ) was observed. In the CGZ, the ratio of length over width of columnar grains was about 10:1. The CGZ and EGZ were induced by different solidification process during the laser-welding process.

Laser-beam welding has a high, focused heat input. The heat generated during LBW is rapidly extracted from the molten fusion zone by the surrounding colder plate. In the vicinity of the fusion boundary, a relatively large thermal gradient contributes to the appearance of columnar grains whereas in the center of the FZ, equiaxed grains form because of a lower temperature gradient.[13] Thereby, a grain morphology transition in the FZ was observed, staring in the CGZ near the fusion line and finishing in the EGZ in the center of the FZ (**Figure 3**).

3.2 Porosity formation

On **Figure 3**, it is also worth noting that no hot cracks are shown in the microstructure of the joint, but some small pores are observed in the BM and FZ, indicated by the arrows in **Figure 3a**. The pore formation is one of the major issues when laser welding magnesium alloys as pores deteriorate the mechanical properties of joints, particularly the tensile strength and elongation.[10] The pore formation can be attributed to many factors such as hydrogen pores,[14] keyhole collapse,[15] initial pores in the BM,[15,16] and capture gases from the air.[17] Owing to the active chemical properties, an Mg alloy is prone to form MgO and H_2 through a chemical reaction with H_2O from the air. Along with the molten-Mg solidification, the H_2 solubility sharply decreases in the solid phase and then pores are formed in the weld bead.

The other important reason for a pore formation is the fact that a molten pool captures the gas from the air during a laser-welding process. In the current work, both the top and bottom surfaces were shielded by argon gas during the laser welding. As mentioned above, the seam of the AZ31B alloy joint was very narrow, about 2 mm (**Figure 2**). Thus, the size of the molten pool was small during the laser welding. In this case, the argon gas could shield the molten pool soundly. Therefore, the pores could not be induced by the hydrogen pores and entrapment gases from the air in this welding process.

In addition, the stability of the keyhole during laser welding, which strongly depends on the surface tension and vapor pressure, is another reason for a pore formation. Generally, Mg-alloys have a more stable keyhole

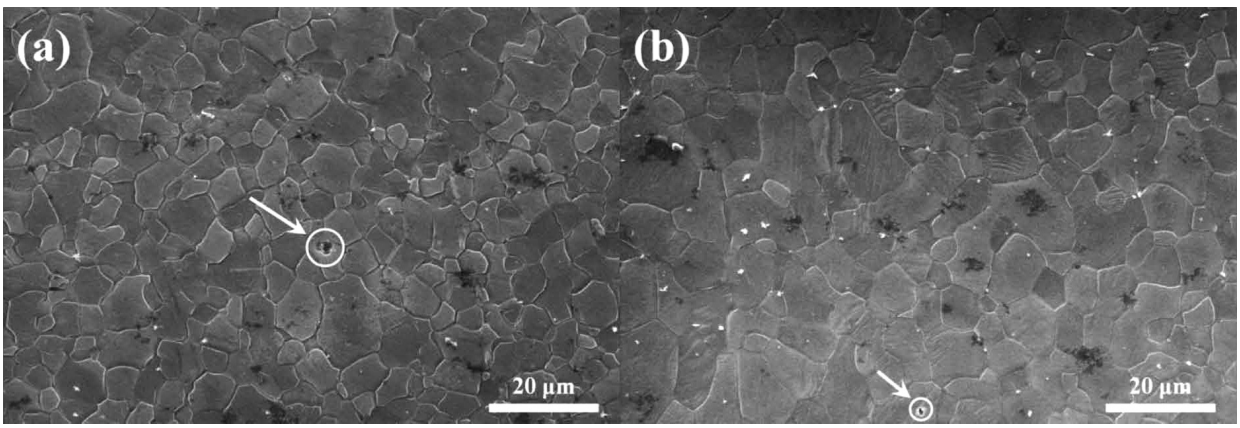

Figure 4: Microstructure of the AZ31B base material

than Al-alloys during a welding process because of their characteristics, including a much higher vapor pressure and a lower surface tension. It is shown in **Figure 2** that after the laser welding, no seam collapse was exhibited in the AZ31B joint. Thereby, an induction of a pore formation due to an unstable keyhole used in this study was not likely to occur.

As indicated by the arrows in **Figures 3a** and **4**, the pores were observed in both the BM and the FZ, demonstrating that the presence of porosity in the FZ can be attributed to the initial small pores in the BM. During the laser-welding process, the pre-existing pores in the BM might grow and coalesce in the molten pool. Similarly, Zhao and Debroy[15] observed that the pre-existing pores in the BM coalesced and expanded in a metal weld during the alloy welding. Wahba et al.[16] also reported that the pre-existing pores in the BM were prone to form pores, which had few chances to escape from the molten weld pool during the laser welding of Mg alloys.

3.3 Grain growth and texture evolution

Another noticeable feature from **Figure 3** is the fact that well-developed columnar grains are nearly perpendicular to the fusion line in the CGZ. This is attributed to the epitaxial growth of the grains adjacent to the solid-liquid line.[18] As the BM could act as the nucleation substrate during the laser welding, the solidification-grain orientation was strongly affected by the BM grains adjacent to the solid-liquid line (indicated by double arrows in the CGZ of **Figure 3b**).[19] In Mg alloys, both <10$\bar{1}$0>-type and *a*-type axes <11$\bar{2}$0> directions of the hcp-crystal lattice are close-packed crystallographic directions, which are the preferred growth orientations during a solidification process.[20,21] Furthermore, the crystal growth within the fusion zone is also significantly influenced by the heat-conduction direction (the thermal gradient) during the solidification process and the maximum value of the thermal gradient is perpendicular to the fusion boundary.[12] Therefore, the grains whose close-packed orientation is parallel to the direction of the maximum thermal gradient, grow more rapidly and restrict other, less favorably oriented grains.

As shown in **Figures 5** and **6**, the texture evolution and microstructure of the weld top surface were analyzed. Contrary to the columnar grains observed in the cross-section of the FZ (**Figure 3**), many equiaxed grains with random orientations were detected on the top surface of the FZ, as illustrated in **Figure 5a**. The BM grains revealed a strong {0001} texture, whose maximum orientation density was about 7.2 (**Figure 5b**) while the maximum grain-orientation density on the top surface of the FZ was only about 2.6, as shown in **Figure 5c**, manifesting almost random grain orientations.

Compared with the welding-pool inside, the welding top surface has a lower thermal gradient *G* and a much faster solidification rate *R* because the shielding-gas flow can carry the heat away rapidly. Thus, a low *G/R* value determined the equiaxed-grain formation on the top surface.[11] Owing to the fast solidification rate, the grains on the top surface of the FZ did not have sufficient time to grow up, and the texture was hardly influenced by the BM grains, having the close-packed crystallographic directions of (<10$\bar{1}$0> and <11$\bar{2}$0>) near the fusion boundary. Consequently, a large number of fine equiaxed grains that had no preferred crystalline orientation were formed on the top surface of the welding seam. Some researchers[11,22,23] claimed that a high thermal gradient would contribute to the growth of columnar grains, while a relatively low thermal gradient could promote the formation of equiaxed grains. These findings are in good agreement with the results observed in **Figures 3** and **5a**. Su et al.[21] studied the electron-beam-welding (EBW) behavior of Mg-Al-based alloys and found that no apparent columnar grains were formed, while many fine equiaxed grains were observed in the Mg-alloy welding bead. Similarly, they also attributed the absence of co-

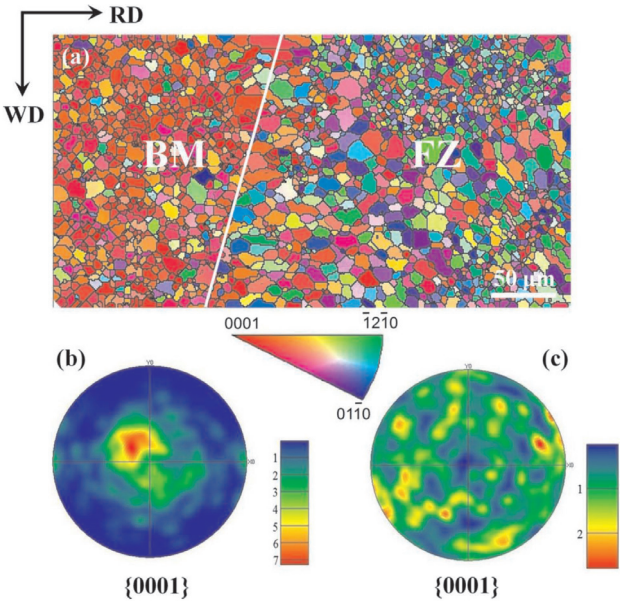

Figure 5: a) Top-surface EBSD map of the laser welded AZ31B joint seam, b) {0001} pole figure of the BM, c) {0001} pole figure of the FZ

Figure 6: Top-surface microstrucutre of the AZ31B joint seam

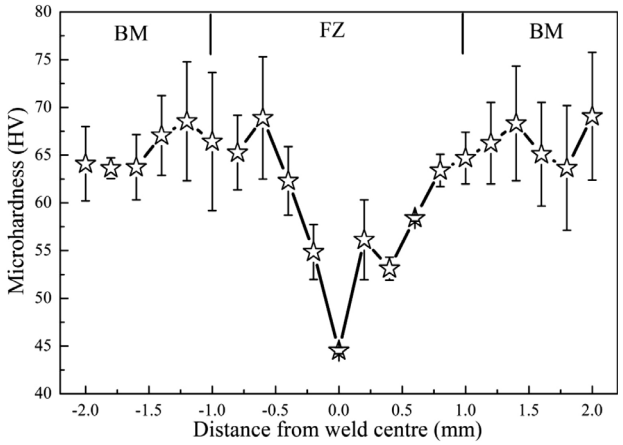

Figure 7: Microhardness distribution across the laser-welded AZ31B joint

lumnar grains to a high cooling rate (a fast solidification rate) during the EBW of Mg-alloys.

3.4 Microhardness distribution

The microhardness profile across the AZ31B joint is illustrated in **Figure 7**, showing that the microhardness changes remarkably between the BM and FZ. The maximum hardness was located in the BM and it was about 68 HV. The lowest hardness value (~ 43 HV) was detected in the center of the FZ, and it was evidently lower than that in the BM. This variation in the microhardness can be attributed to the microstructural changes in the BM and FZ.

According to the Hall-Petch relationship,[24] grain coarsening can reduce the hardness of an alloy. In contrast, the Orowan hardening mechanism indicates that a large number of hard precipitate particles within a matrix can improve the hardness of an alloy.[25] As shown in **Figure 3**, the grain coarsening of α-Mg was observed in the FZ of the AZ31B welded joints. Furthermore, a very small amount of precipitates appeared in the AZ31B alloy joints. Consequently, the grain-coarsening mechanism dominated the microhardness distribution in this research.

4 CONCLUSIONS

Laser welding of an AZ31B Mg alloy was conducted using a low-power pulsed Nd:YAG laser. The metallurgical characteristics of the AZ31B alloy joint were systematically investigated in the present work. Owing to different thermal gradients, a grain-morphology transition was observed in the FZ, taking place from the CGZ near the fusion line towards the EGZ in the center of the FZ. Some small pores were observed in the FZ and believed to be caused by the pre-existing pores in the BM. An epitaxial growth of the columnar grains in the FZ, which were nearly perpendicular to the solid-liquid boundary, was observed in the cross-section of the FZ. This was caused by the maximum temperature gradient and the close-packed crystallographic directions (<10$\bar{1}$0> and <11$\bar{2}$0>) of the Mg alloys. Being different from the columnar grains in the welding pool, fine equiaxed grains with random orientations were formed on the top surface of the welding bead due to a relatively high cooling rate and a low G/R value on the top surface. Because of apparent grain coarsening of the FZ, the minimum hardness value (~ 43 HV) was detected in the center of the FZ and it was clearly lower than that of the BM (~ 68 HV).

Acknowledgement

This work was supported by the Natural Science Foundation of Shandong Province, China (grant no. ZR2018BEE013), the National Key Research and Development Plan of China (grant no. 2017YFB0103904, 2016YFB0701202), the Shandong Province Key Research and Development Plan, China (grant no. 2017CXGC0404, 2016ZDJS02A09), and the Youth Foundation of Shandong Academy of Sciences, China (grant no. 2016QN015).

5 REFERENCES

[1] M. K. Kulekci, Magnesium and its alloys applications in automotive industry, Int. J. Adv. Manuf. Technol., 39 (**2008**) 9, 851–865, doi:10.1007/s00170-007-1279-2

[2] M. Easton, A. Beer, M. Barnett, C. Davies, G. Dunlop, Y. Durandet, S. Blacket, T. Hilditch, P. Beggs, Magnesium alloy applications in automotive structures, JOM, 60 (**2008**) 11, 57–62, doi:10.1007/s11837-008-0150-8

[3] G. S. Frankel, Magnesium alloys: Ready for the road, Nat. Mater., 14 (**2015**) 12, 1189–1190, doi:10.1038/nmat4453

[4] H. T. Liu, J. X. Zhou, D. Q. Zhao, Y. T. Liu, J. H. Wu, Y. S. Yang, B. C. Ma, H. H. Zhuang, Characteristics of AZ31 Mg alloy joint using automatic TIG welding, Int. J. Miner. Metall. Mater., 24 (**2017**) 1, 102–108, doi:10.1007/s12613-017-1383-8

[5] J. Shen, K. Liu, Y. Li, S. Z. Li, L. B. Wen, Effects of fluxes on distribution of SiC particles and microstructures and mechanical properties of nanoparticles strengthening A-TIG (NSA-TIG) welded magnesium alloy joints, Sci. Technol. Weld. Joining, 18 (**2013**) 5, 404–413, doi:10.1179/1362171813Y.0000000112

[6] C. M. Lin, H. L. Tsai, C. L. Lee, D. S. Chou, S. F. Lee, J. C. Huang, J. W. Huang, Influence of CO2 laser welding parameters on the microstructure, metallurgy, and mechanical properties of Mg-Al alloys, Int. J. Miner. Metall. Mater., 19 (**2012**) 12, 1114–1120, doi:10.1007/s12613-012-0679-y

[7] K. Yan, J. Su, Y. Zhao, Microstructure and mechanical properties of the laser-welded Mg-3Nd-0.2Zn-0.4Zr (NZ30K) magnesium alloy, Opt. Laser Technol., 93 (**2017**), 109–117, doi:10.1016/j.optlastec.2017.02.002

[8] M. Gao, S. Mei, Z. Wang, X. Li, X. Zeng, Process and joint characterizations of laser–MIG hybrid welding of AZ31 magnesium alloy, J. Mater. Process. Technol., 212 (**2012**) 6, 1338–1346, doi:10.1016/j.jmatprotec.2012.01.011

[9] D. Wang, J. Shen, L. Z. Wang, Effects of the types of overlap on the mechanical properties of FSSW welded AZ series magnesium alloy joints, Int. J. Miner. Metall. Mater., 19 (**2012**) 3, 231–235, doi:10.1007/s12613-012-0543-0

[10] X. Cao, M. Jahazi, J. P. Immarigeon, W. Wallace, A review of laser welding techniques for magnesium alloys, J. Mater. Process.

Technol., 171 (**2006**) 2, 188–204, doi:10.1016/j.jmatprotec.2005.06.068

[11] S. M. Chowdhury, D. L. Chen, S. D. Bhole, E. Powidajko, D. C. Weckman, Y. Zhou, Microstructure and Mechanical Properties of Fiber-Laser-Welded and Diode-Laser-Welded AZ31 Magnesium Alloy, Metall. Mater. Trans. A, 42 (**2011**) 7, 1974–1989, doi:10.1007/s11661-010-0574-y

[12] R. S. Coelho, A. Kostka, H. Pinto, S. Riekehr, M. Koçak, A. R. Pyzalla, Microstructure and mechanical properties of magnesium alloy AZ31B laser beam welds, Mater. Sci. Eng. A, 485 (**2008**) 1–2, 20–30, doi:10.1016/j.msea.2007.07.073

[13] S. Kou, Y. Le, Welding parameters and the grain structure of weld metal – A thermodynamic consideration, Metall. Trans. A, 19 (**1988**) 4, 1075–1082, doi:10.1007/bf02628392

[14] X. Cao, M. Xiao, M. Jahazi, J. P. Immarigeon, Continuous Wave ND:YAG Laser Welding of Sand-Cast ZE41A-T5 Magnesium Alloys, Mater. Manuf. Processes, 20 (**2005**) 6, 987–1004, doi:10.1081/AMP-200060436

[15] H. Zhao, T. Debroy, Pore formation during laser beam welding of die-cast magnesium alloy AM60B – mechanism and remedy, Weld. J., 80 (**2001**) 8, 204–210

[16] M. Wahba, M. Mizutani, Y. Kawahito, S. Katayama, Laser welding of die-cast AZ91D magnesium alloy, Mater. Des., 33 (**2012**), 569–576, doi:10.1016/j.matdes.2011.05.016

[17] L. Liu, G. Song, G. Liang, J. Wang, Pore formation during hybrid laser-tungsten inert gas arc welding of magnesium alloy AZ31B – mechanism and remedy, Mater. Sci. Eng. A, 390 (**2005**) 1–2, 76–80, doi:10.1016/j.msea.2004.07.067

[18] L. Liu, L. Xiao, J. C. Feng, Y. H. Tian, S. Q. Zhou, Y. Zhou, Resistance Spot Welded AZ31 Magnesium Alloys, Part II: Effects of Welding Current on Microstructure and Mechanical Properties, Metall. Mater. Trans. A, 41 (**2010**) 10, 2642–2650, doi:10.1007/s11661-010-0339-7

[19] L. Xiao, L. Liu, Y. Zhou, S. Esmaeili, Resistance-Spot-Welded AZ31 Magnesium Alloys: Part I. Dependence of Fusion Zone Microstructures on Second-Phase Particles, Metall. Mater. Trans. A, 41 (**2010**) 6, 1511–1522, doi:10.1007/s11661-010-0197-3

[20] S. Kou, Welding Metallurgy, 2nd ed., Wiley, Hoboken, 2003, 175

[21] S. F. Su, H. K. Lin, J. C. Huang, N. J. Ho, Electron-beam welding behavior in Mg-Al-based alloys, Metall. Mater. Trans. A, 33 (**2002**) 5, 1461–1473, doi:10.1007/s11661-002-0069-6

[22] L. Commin, M. Dumont, R. Rotinat, F. Pierron, J. E. Masse, L. Barrallier, Texture evolution in Nd:YAG-laser welds of AZ31 magnesium alloy hot rolled sheets and its influence on mechanical properties, Mater. Sci. Eng. A, 528 (**2011**) 4–5, 2049–2055, doi:10.1016/j.msea.2010.11.061

[23] Y. J. Quan, Z. H. Chen, X. S. Gong, Z. H. Yu, Effects of heat input on microstructure and tensile properties of laser welded magnesium alloy AZ31, Mater. Charact., 59 (**2008**) 10, 1491–1497, doi:10.1016/j.matchar.2008.01.010

[24] B. S. Naik, D. L. Chen, X. Cao, P. Wanjara, Microstructure and Fatigue Properties of a Friction Stir Lap Welded Magnesium Alloy, Metall. Mater. Trans. A, 44 (**2013**) 8, 3732–3746, doi:10.1007/s11661-013-1728-5

[25] J. F. Nie, Effects of precipitate shape and orientation on dispersion strengthening in magnesium alloys, Scr. Mater., 48 (**2003**) 8, 1009–1015, doi:10.1016/S1359-6462(02)00497-9